Histopathological evaluation of prostate specimens after thermal ablation may be confounded by the presence of thermally fixed cells.

Eemil Yli-Pietilä

Syventävien opintojen kirjallinen työ

Turun yliopisto

Lääketieteellinen tiedekunta

Urologia

Tammikuu 2020

TURUN YLIOPISTO
Kliininen laitos, Lääketieteellinen tiedekunta
Syventävien opintojen kirjallinen työ, tiivistelmä
Ohjaajat: Otto Ettala, Mikael Anttinen

YLI-PIETILÄ, EEMIL: Histopathological evaluation of prostate specimens after thermal ablation may be confounded by the presence of thermally fixed cells.

Tammikuu 2020

_ _

TULSA (transurethral ultrasound ablation) on kokeellinen magneettikuvantamisohjattu hoitomuoto eturauhassairauksien hoitoon. Sen vaikutus perustuu virtsaputken kautta lähetettäviin ultraääniaaltoihin, jotka kuumentavat eturauhaskudosta. Eturauhaskudoksen lämpötilan nousu yli 55 asteen aiheuttaa välittömän koagulaationekroosiin, johon menetelmän terapeuttinen vaikutus perustuu. Hoidon aikana seurataan reealiaikaisesti kohdekudoksen lämpötilamuutoksia lämpöherkillä magneettikuvilla, MRI-termometrialla, jonka avulla voidaan varmistaa haluttu lämpövaikutus eturauhasessa. Nopea ja korkea lämpötilan nousu saattaa kuitenkin aiheuttaa termofiksaatioksi kutsutun ilmiön, jossa kudos vaikuttaa morfologisesti elinkelpoiselta, vaikka todellisuudessa kudos saattaa olla tuhoutunut. Tämän tutkimuksen tarkoitus oli määrittää epäilyjen termofiksoituneiden eturauhasalueiden elinkelpoisuus ja kuvailla näiden immunoprofiilia.

Prospektiivisissa tutkimuksessa (ClinicalTrials.gov: NCT03350529) 6 potilaan eturauhassyövät hoidettiin TULSA-hoidolla. Jokaisella potilaalla oli magneettikuvantamisella todennettu ja biopsiavarmennettu eturauhassyöpä ja jokaiselle potilaalle tehtiin gadolinium-tehosteinen magneettikuvaus ja eturauhasen poistoleikkaus kolme viikkoa TULSA-hoidon jälkeen. Leikkauksessa poistetuille eturauhasille tehtiin normaali histopatologinen tutkimus. Mikäli epävarmuus täydellisestä nekroosista hematosykliini-eosiinivärjäyksen jälkeen jäi, tehtiin immunohistokemiallinen värjäys. Ablaatioalueen vertailukohtana morfologian tutkimisessa käytettiin eturauhasen lämpövaikutukselta välttynyttä kudosta.

Yhdellä potilaalla todettiin termofiksaatio. Alue sijaitsi ablaatioalueen sisällä kohdassa, jossa MRI-termometriassa lämpötila oli ollut korkeimmillaan. Alueen verisuonitus oli myös täysin hävinnyt gadolinium-tehosteisissa magneettikuvissa. Ympärillä oleva kudos oli hematosykliini-eosiinivärjäyksessä nekrotisoitunut. Elinkelpoiselta näyttäneen kudoksen immunoprofiilissa paljastui termofiksaatioon sopivia värjäysmallin muutoksia. Tärkeimpänä todisteena termofiksaatiosta oli Cam5.2- vasta-aineella havaittu cytokeratin 8 -värjäyksen negatiivisuus. Laaja kirjallisuuskatsaus tukee näitä havaintoja eturauhasesta ja muista kudoksista havaituista termofiksaatioista.

Termofiksoituneet solut siis voivat säilyttää morfologiansa hematosykliini-eosiinvärjäyksessä. Mikäli termofiksoituneita alueita ei tunnisteta tai ei tutkita immunohistokemiallisesti, voi lopputuloksena olla väärä päättely hoidon epäonnistumisesta. Aikasempaan kirjallisuuteen ja tähän tutkimukseen perustuen Cam5.2. värjäys cytokeratin 8:lle vaikuttaa olevan käytännöllinen ja luotettava apuväline termofiksoituneiden solujen erottamiseksi elinkelpoisista soluista.

Asiasanat: eturauhassyöpä, fokaaliterapia, termofiksaatio, TULSA

HISTOPATHOLOGICAL EVALUATION OF PROSTATE SPECIMENS AFTER THERMAL ABLATION MAY BE CONFOUNDED BY THE PRESENCE OF THERMALLY-FIXED CELLS

Mikael Anttinen [a, *], Eemil Yli-Pietilä [b], Visa Suomi [c], Pietari Mäkelä[c], Teija Sainio[c], Jani Saunavaara [c], Lauri Eklund [e], Roberto Blanco Sequeiros [b], Pekka Taimen [e, +], Peter J. Boström [a, +]

[a] Department of Urology, Turku University Hospital,

[b] Faculty of Medicine, University of Turku,

[c] Department of Diagnostic Radiology, University of Turku, Finland,

[d] Medical Imaging Centre of Southwest Finland, Turku University Hospital, Turku, Finland,

[e] Institute of Biomedicine, University of Turku and Department of Pathology, Turku University Hospital, Turku, Finland

[*] Corresponding author Department of Urology, Turku University Hospital, email: mhjant@utu.fi

[+] These authors have contributed equally in this manuscript

Emil Yli-Pietilä, ehmyli@utu.fi; Visa Suomi, visa.suomi@tyks.fi; Pietari Mäkelä, pjmake@utu.fi; Teija Sainio, teija.sainio@tyks.fi; Jani Saunavaara, jani.saunavaara@tyks.fi; Lauri Eklund, lajuek@utu.fi; Roberto Blanco Sequeiros, roberto.blanco@tyks.fi;Pekka Taimen, pekka.taimen@tyks.fi; Peter J. Boström, peter.bostrom@tyks.fi.

KEYWORDS: focal therapy, clinical trials-thermal ablation, noninvasive thermometry, physiological effects of hyperthermia, ultrasound

Number of words (abstract): 250

Number of words (text): 3832

Number of tables: 1

Number of figures: 4

Number of references: 53

Supplemental material: 1 (Table S1)

ABSTRACT

BACKGROUND

Prostate cancer can be eradicated with heat-exposure. However, high and rapid temperature elevations may cause thermofixation giving the appearance of viable tissue. The purpose was to characterize the immunoprofile and evaluate the viability of prostate regions with suspected thermofixation.

MATERIAL AND METHODS

A prospective, **ethics-approved** and registered study **(NCT03350529)** enrolled six patients with MRI-visible, biopsy-concordant prostate cancer to undergo lesion-targeted MRI-guided transurethral ultrasound ablation (TULSA) followed by radical prostatectomy at 3 weeks, to evaluate the accuracy and efficacy of TULSA with whole-mount-histology as a reference standard. If ambiguity about complete necrosis within the ablated region remained after hematoxylin-eosin-staining, viability was assessed by immunohistochemistry. Treatment day MRI-thermometry and 3-week contrast-enhanced MRI post-TULSA were examined to assess ablation success and correlation with histopathology.

RESULTS

One patient presented with an apparently viable sub-region inside the ablated area, surrounded by necrosis on H&E-staining, located where temperature was highest on MRI-thermometry and tissues completely devascularized on MRI. Immunoprofile of the apparently viable tissue revealed **changes in staining patterns** suggesting thermofixation; the most significant evidence was the negative cytokeratin 8 staining **detected with Cam5.2 antibody**. A comprehensive literature review supports these observations of thermofixation with similar findings in prostate and other tissues.

CONCLUSION

Thermally-fixed cells can sustain morphology on H&E staining. Misinterpretation of treatment failure may occur, if this phenomenon is not recognized and immunohistochemistry performed. Based on the previous literature and the current study, **Cam5.2 staining for** cytokeratin 8 appears to be a practical and reliable tool for distinguishing thermally-fixed from viable cells.

INTRODUCTION

Standard therapies for clinically significant localized prostate cancer (PCa) including radical prostatectomy (RP) and radiation therapy (RT) provide proven cancer control with improved survival [1-3], but carry the risk of treatment-related adverse effects to genitourinary and bowel function [4,5]. For selected patients, minimally invasive focal ablative therapies (FT) may offer an effective and less morbid alternative for PCa management. While FTs are increasingly utilized in PCa management, they are considered experimental due to insufficient evidence confirming their longer-term oncological efficacy [6].

Most FTs in clinical practice use thermal energy to ablate prostate tissue, typically heating prostate tissue with radiofrequency, microwave, laser, or high intensity focused ultrasound (HIFU) energy [7]. Some modern heat-based treatment systems exploit magnetic resonance imaging (MRI) for detecting and visualizing PCa-lesions and guiding therapy into targeted regions [8-10].

MRI-guided transurethral ultrasound ablation (TULSA) is a novel therapy method for treating organ-confined PCa which has obtained promising results in terms of feasibility, safety and early efficacy [11-13]. TULSA delivers directional ultrasound from within the prostatic urethra to ablate prostate tissue [14]. By rapidly raising and maintaining elevated tissue temperatures above 55°C, target tissue is destroyed primarily by undergoing acute coagulation necrosis and secondarily due to

delayed thermal injury [15-18]. TULSA employs MRI-thermometry allowing real-time temperature changes to be monitored and subsequently used to control therapy so that precise conformal ablative volumes can be achieved [19-22]. The ablated volume is visualized post-treatment on contrast enhanced MRI as a non-perfused-volume (NPV) indicating complete irreversible cell death [23-26]. The histopathological analyses of immediate and 3-week post-TULSA RP-specimens have revealed accurate and precise ablation pattern with sharp demarcation of thermal injury. These treatment features of TULSA enable controlled ablation of prostate tumors with potentially reduced risk of damaging surrounding vulnerable tissues including the neurovascular bundles (NVB), bladder neck, pelvic floor muscles, and rectal wall [11-13].

Although FTs appear promising for safe and efficient management of PCa, they continue to face challenges in determining how to monitor treatment efficacy and follow-up oncological outcome. Currently, the recommended follow-up measures after FT include prostate specific antigen (PSA), prostate MRI, and biopsy [6]. However, histopathological evaluation of prostate specimens after thermal ablation can be challenging due to various tissue changes related to heat-induced tissue destruction [16,17,27]. In general, three zones with a spectrum of specific morphological changes have been distinguished including a **thermal fixation zone (TFZ)**, a coagulative necrosis zone (CNZ), and a margin zone (MZ) [17].

A high and rapid temperature rise in tissue may cause thermal fixation that retains tissue morphology in hematoxylin-eosin (H&E) staining suggesting untreated viable tissue [16,17,28-39]. Several studies have demonstrated the appearance of thermal fixation in various human tissues [32,37-39], including two treat-and-resect-studies in RP-specimens after thermal ablation with HIFU [16] and laser [36].

In clinical practice, thermally-fixed cells that appear viable on H&E after thermal ablation can confound histological assessment. If ancillary staining to identify thermofixation is not performed, this effect may lead to misdiagnosis of treatment failure and subsequently to incorrect treatment decisions.

Concept of thermal dose and mechanisms of cell death due to heat exposure

Therapeutic ultrasound generates heat by a thermoviscous effect where the mechanical energy of a propagating ultrasound wave is absorbed by tissue and converted into heat. The temperature rise caused by heating is dependent on the frequency and intensity of the ultrasound field as well as the physical properties of tissue including perfusion rate, thermal conduction and attenuation. These tissue properties are also temperature dependent, which further affects the heating efficacy. For instance, in prostate the perfusion rate has been shown to significantly increase during hyperthermia treatments [40], which reduces the temperature and consequently tissue thermal damage.

Thermal damage induced to tissue cells due to heating is not only dependent on temperature but also on the duration of heat exposure. To quantify the cumulative effect of both temperature and time on cell injury, the metric of thermal dose was developed by Sapareto and Dewey [41]:

$$\mathrm{CEM}_{43} = \int_0^{t_{\mathrm{end}}} R^{43-T(t)} \mathrm{d}\, t$$

where t_{end} is heating duration in minutes, T is temperature in ˚C, and R is 0.25 for temperatures below 43 ˚C and 0.5 otherwise. The idea of thermal dose is to convert any time-temperature combination of different thermal exposures to 'cumulative equivalent-minutes' at the temperature of 43 ˚C (CEM_{43}) which allows comparison using the same quantitative scale. By the definition of thermal dose, each one-degree increase in temperature above 43 ˚C halves the required heating duration for the same effective dose. The relationship between time and temperature for cell damage is therefore exponential, which has also been demonstrated in experimental studies [41,42]. For example, a heat exposure of one minute at 51 ˚C has the same thermal dose as 256 minutes at 43 ˚C (i.e., 256 CEM_{43}). Thus, thermal dose offers a simple but effective metric for determining treatment parameters for hyperthermia and thermal ablation therapies in clinical use.

The thermal dose scale does not require that different tissues have the same sensitivity to heat, and therefore, thresholds for cell damage and death due to heat exposure can be determined individually for each tissue type. Generally, a thermal dose of 240 CEM_{43} has been accepted as the threshold for cell death in thermal ablation modalities, such as HIFU therapy [43,44], where relatively rapid and high temperature elevations are used. However, some cell types are more resistant to heat than others, and therefore, the thermal dose required for cell damage or death should be tissue-specific [42,45]. The differences in tissue thermal sensitivities are due to several reasons including the characteristics of protein structure, and the kinetics of repair and replacement processes [42]. For prostate tissue it has been shown that thermal dose below 50 CEM_{43} causes no damage, 80 CEM_{43} causes minor damage and 240 CEM_{43} results in complete thermal coagulation [45].

It should be noted that there are a number of other factors which also affect the usage of thermal dose for measuring tissue damage. Tissues that have previously been exposed to heat might have acquired resistance to subsequent exposures at elevated temperatures (i.e., thermotolerance) [46],

which in turn increases their thresholds for cell damage in terms of thermal dose. In addition, since the thermal dose metric was derived for the purpose of clinical hyperthermia treatments, there may be extrapolation inaccuracies when applying the metric to other thermal therapies where very low or very high temperatures are typical (i.e., outside the range of 39 - 57 ˚C) [42,47]. It is also assumed that the value of *R* is constant across a range of tissues with the breakpoint occurring at 43 ˚C, which might not always be the case [42,48]. Lastly, most of the data used to determine thermal dose thresholds in different tissues has been obtained from either animal or human cell line studies, which might not directly relate to the thermal sensitivity of human tissues *in vivo* [42,45].

The term 'thermal necrosis' generally refers to the stage of tissue after irreversible cell death due to heat exposure. However, necrosis only happens after cell death and thus the terms should not be used interchangeably [49]. Cell death due to thermal exposure can occur via multiple pathways. When relatively low temperatures below 60 ˚C are used, the primary mechanism of cell death is apoptosis where the internal cell structure is destroyed via a controlled process and without inflammation. In apoptotic cells, the nucleus of the cell is self-destroyed and its DNA is degraded by endonucleases [50]. At higher temperatures above approximately 60 ˚C, rapid protein denaturation occurs which leads to coagulative thermal necrosis (i.e., thermal ablation) [15]. At these 'high temperatures' collagen fibres gain enough energy to irreversibly transform from a uniform helical-state to a more random-state of lower organization [51,52].

Biology of thermal fixation

When the local temperature rise in tissue is sufficiently high and rapid, a process known as thermal fixation may also occur [32,35]. Thermally-fixed cells exhibit no visible morphological changes in traditional light microscopy, but closer investigation with scanning electron microscopy has shown

them to lack nuclear membranes and organelle structures indicating irreversible cell death [37]. Thermal fixation appears to result from denaturation of the structural and enzymatic protein constituents of tissue, so that they are able to resist the typical repair/breakdown pathways of the body [32,34]. Therefore, thermally-fixed cells maintain their cytologic staining characteristics and preserved nuclear chromatin, which gives a histological staining appearance similar to viable cells [37]. This might lead to misinterpretation of histopathology results from thermal ablation therapies, when certain types of stains are used [16,37].

Objective

The purpose of this study was to characterize the immunoprofile and evaluate the viability of morphologically unaltered sub-regions of prostatic tissue within regions of coagulative necrosis on H&E staining after thermal ablation with TULSA. Multimodal analysis including treatment day MRI-thermometry, post-TULSA 3-week NPV and comprehensive immunohistochemistry (IHC) were utilized for the assessment of the true nature and viability of the ablated tissue suspected to present thermal fixation. These results were contextualized by performing a comprehensive review of the applicable literature.

MATERIAL AND METHODS

Study Design

A prospective, registered (ClinicalTrials.gov Identifier: NCT03350529), single-center clinical phase-I study consented and enrolled 6 patients with MRI-visible, biopsy-concordant localized PCa to undergo lesion-targeted TULSA (TULSA-PRO, Profound Medical Inc., Toronto, Canada; integrated into a 3T MR-system Ingenia 3.0T, Philips Healthcare, Best, Netherlands), followed by robot-assisted laparoscopic radical prostatectomy (RALP) at 3 weeks. The treat-and-3-week-resect-setting enabled histological assessment of TULSA accuracy and efficacy including delayed thermal injury, but necessitated conservatively defined ablation zones to preserve surgical outcomes. In the vicinity of the neurovascular bundles (NVB), safety margins up to 3 mm were applied regardless of tumor extent, based on the concern that necrosis may migrate beyond the region of acute coagulation necrosis [18], potentially compromising the subsequent nerve-sparing RALP. All of the resected RALP specimens were formalin-fixed and paraffin-embedded for histopathological evaluation. **The study protocol was approved by the local Ethics committee of the Hospital District of Southwest Finland, and written informed consent was obtained from all participants.**

Initial histopathology of the whole-mount sections included H&E and IHC stainings. The evaluation was first performed under conventional light microscopy **on glass slides and thereafter also on digital whole slide images.** If complete and irreversible cell death of the ablated region remained ambiguous after H&E staining, comprehensive IHC was performed to characterize the immunoprofile and assess the viability of these regions. **The staining pattern of the prostate**

glandular epithelium was assessed for CAM5.2 (cytokeratin 7 and 8), p16, and androgen receptor. AMACR (Alpha-methylacyl-Coa racemase/P504S) was utilized to distinguish malignant glands from benign glands. Proliferation activity was assessed with Ki-67 staining and thermal vascular damage was assessed with antibody to Factor VIII (von Willebrand Factor, vWF). **All slides were examined by the same uropathologist with 10 years of experience in uropathology. The selected slides covering the ablation area were also examined by another uropathologist with more than 30 years of experience.**

Data on treatment day MRI-thermometry and post-TULSA NPV at 3 weeks were also exploited to assess success of the ablation and the concordance of MRI findings with histopathology.

Histology and Immunohistochemistry

The RALP specimens were fixed in 10 % formalin and cut into approximately 5 mm sections with free hand as follows: apex and base in coronal plane, seminal vesicles in sagittal and mid-gland in transverse plane perpendicular to the long axis of the urethra. The entire material was embedded in paraffin using whole-mount macro cassettes. Two 5 μm sections from each block were cut for H&E staining and additional sections from selected blocks for IHC using BenchMark XT and ULTRA IHC/ISH automated slide staining instruments (Ventana Medical Systems, Tucson, Arizona, USA). All H&E slides were examined. The detailed list of utilized antibodies is shown in supplementary Table S1.

Author	Therapy device	Material	Methods				Validation of thermal fixation
			SS	HP	IHC	Others	
Van Leenders et al (2000)	HIFU	9 human prostate whole glands in vivo		H&E; uranyl acetate; lead citrate	CK8; anti-PSA; panCK; Ki67	Electron microscopy	Thermal fixation indicated by H&E in 6 prostates; non-viability confirmed by CK8 negativity and electron microscopy
Bhowmick et al (2004)	Heating with copper block	10 human prostate tissue samples in vitro		H&E		Fluorescence microscope (EthD-2 and Hoechst 33342 dyes)	Thermal fixation indicated by H&E; non-viability confirmed by fluorescence microscopy
Boyes et al (2007)	Transurethral ultrasound	7 canine prostate whole glands in vivo	TTC	H&E		CE-MRI	Non-viability confirmed by TTC unstaining; thermally fixated in H&E-staining
Lindner et al (2010)	FLA	4 human prostate whole glands in vivo		H&E	CK8 (CAM 5.2)	CE-MRI	Thermal fixation indicated by H&E; non-viability confirmed by CK8 negativity and CE-MRI
Stafford et al (2010)	LITT	7 canine prostate whole glands in vivo		H&E	vWF	CE-MRI	Thermal fixation in every prostate in H&E; non-viability confirmed by vWF
Germer et al (1998)	LITT	55 rabbit liver whole glands in vivo		H&E; silver nitrate; azan		CE-MRI	Non-viability indicated by morphology with H&E; non-viability confirmed by CE-MRI
Coad et al (2003)	RFA	4 human liver whole glands in vivo		H&E		CE-MRI: CE-CT	Thermal fixation in every liver in H&E; non-viability confirmed by CE-MRI or CE-CT
Leslie et al (2008)	HIFU	6 human liver whole glands in vivo	TTC	H&E	Factor VIII	CE-MRI	Thermal fixation in 1 indicated by lack of post-mortem autolysis in morphology; non-viability confirmed by Factor VIII and CE-MRI
Courivaud et al (2014)	HIFU	4 + 5 swine liver whole glands in vivo*		H&E		CE-MRI	Thermal fixation in 7 livers in H&E; non-viability confirmed by CE-MRI and by presence of foreign-body giant cells
Hennings et al (2009)	CITT	8 nipples of one swine in vivo; 8 rabbit VX2 carcinomas in vivo	TTC	H&E	Anti-PCNA	Autofluorescence microscopy	Thermal fixation indicated by H&E; non-viability confirmed by TTC and autofluorescence microscopy
He et al (2004)	MW thermal therapy	5 + 7 + 8 porcine kidneys in vitro or in vivo **		H&E			Thermal fixation in every kidney; non-viability indicated by morphology with H&E
Wu et al (2006)	HIFU	23 human breast whole organ in vivo	NADH	Uranyl acetate; lead citrate; H&E	biotin-streptavidin-peroxidase; CA15-3; VEGF	Electron microscopy	Thermal fixation in 11 breast tumors indicated by H&E; non-viability confirmed by NADH and electron microscopy

Table 1: Previous literature of thermal fixation

Therapy device: HIFU=high intensity focused ultrasound, LITT=laser interstitial thermal therapy, FLA=focal laser ablation, RFA=radiofrequency ablation, CITT=conductive interstitial thermal therapy, MW= microwave; Supravital staining (SS): TTC=triphenyl tetrazolium chloride, NADH=nicotinamide adenine dinucleotide; Histopathology (HP): H&E=hematoxylin-eosin; ICH=immunohistochemistry: CK=cytokeratin, PSA=prostate specific antigen, vWF=von Willebrandt factor, PCNA=proliferating nuclear antigen, CE-MRI=contrast-enhanced magnetic resonance imaging
*4 ablated and euthanized after immediate MR; 5 in survival study, euthanized after 1wk MRI
**4 animals, 5 kidneys in vitro; 6 animals, 7 kidneys in vivo 2h perfusion; 4 animals, 8 kidneys in vivo 7d perfusion

Histological Image Analysis

All H&E and IHC slides were scanned with NanoZoomer S60 (Hamamatsu Photonics, Hamamatsu, Japan) using the NDP.scan software (v. 3.2.12) and 20x scanning mode. Representative areas of each slide were captured with specific magnification pointing out region of interest in NDP.view2 software in which annotation were performed for all the slides. Two thermal damage boundaries were contoured: 1) the outer boundary of complete necrosis (complete and irreversible cell death) and 2) the outer limit of thermal injury (OLTI), outside which there was no visual evidence of thermal damage. The zone inside the complete necrosis boundary was defined as the coagulation necrosis zone (CNZ), and the zone between complete necrosis and the OLTI was defined as the margin zone (MZ).

RESULTS

Study subjects

All of the 6 enrolled participants completed the study, and one of them presented with apparently viable tissue within the continuous area of coagulation necrosis on initial H&E-staining (Figure 1). For this patient, comprehensive IHC was performed. The baseline clinical, MRI, and tumor characteristics of this case are summarized in Figure 2a and described in detail below.

Figure 1. Annotated H&E stained axial whole-mount slide mid from the RALP specimen from every study patient. All patients except patient four presented complete coagulation necrosis of the targeted tumor: the complete irreversible cell death inside the red boundary (CNZ) and margin zone between red and blue boundaries (MZ). Patient 4 presented thermally-fixed viable-looking cells within green boundaries. Black contoured regions present outfield (outside treatment boundaries) residual prostate cancer.

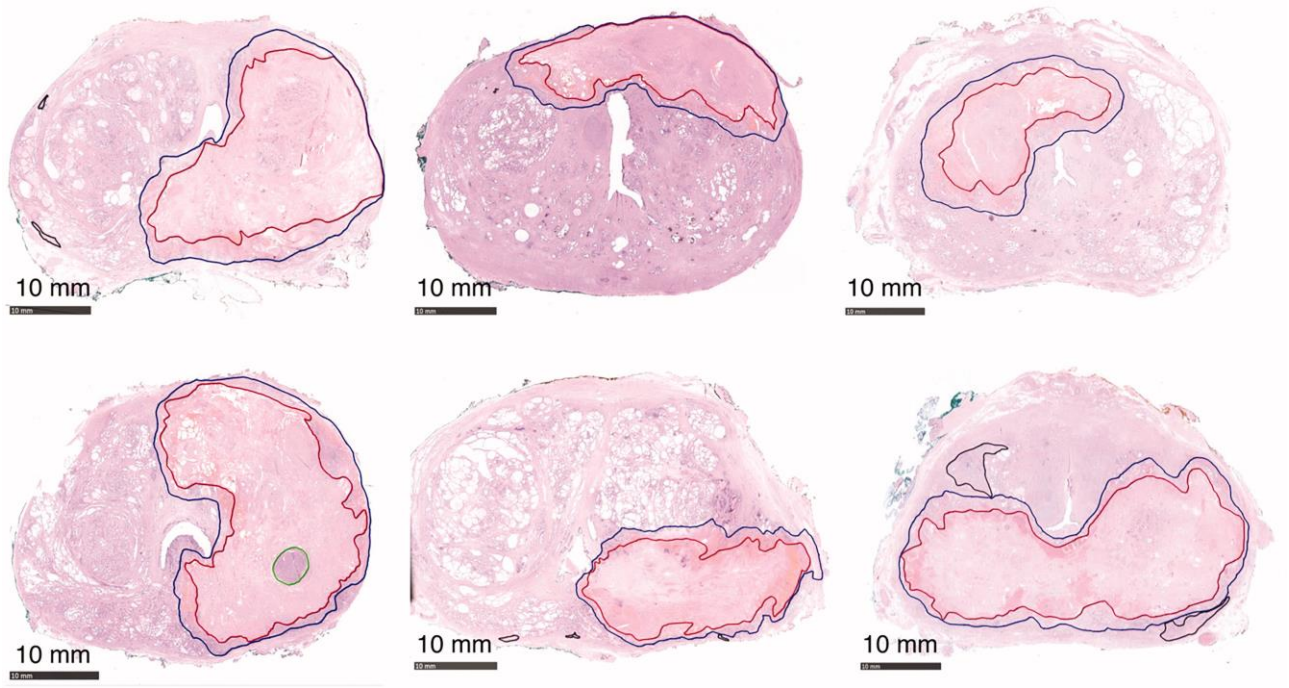

Figure 2. (A) Patient 4: A 70-year-old (ECOG 0, prostate volume 51 cc, BMI 30) Caucasian man without urinary symptoms and with elevated PSA level 36 ng/mL underwent pre-biopsy prostate MRI showing a left lobe situated 5.1 cc PIRADS 5 lesion in the close contact with prostate capsule. Axial, coronal and sagittal T2-weighted images on top panel (left to right in order); diffusion weighted and apparent diffusion coefficient images on bottom panel (left and middle) from the PIRADS 5 lesion. All the MRI-targeted 6-core biopsies confirmed Gleason Score 4 + 3=7 PCa within the dominant lesion with cancer core length of 53 mm. The whole-body contrast-enhanced computer tomography (CT) and bone scintigraphy were both negative for metastasis. F18-prostate-specific membrane antigen (PSMA) positron emission tomography-CT excluded distant metastasis and showed an intensive PSMA-uptake with standardized uptake value maximum of 81.1 g/mL in the left lobe of the prostate concordant with the MRI (on bottom panel left). (B) Immediate post-treatment overlay images have been demonstrated from the active element of the patient 4: on the left targeted region; on the middle maximum temperature and thermal dose maps and on the right non-perfused volume (NPV). Yellow boundary demonstrates targeted region on treatment planning, purple 240 CEM43 isodose boundary and green 55° isotherm boundary. (C) This figure presents post-TULSA NPV on sagittal and axial images at 3 weeks just prior to RALP procedure and the sliced RALP specimen on the right, in which thermal damage region is clearly identified as the dark regions on the gross specimen.

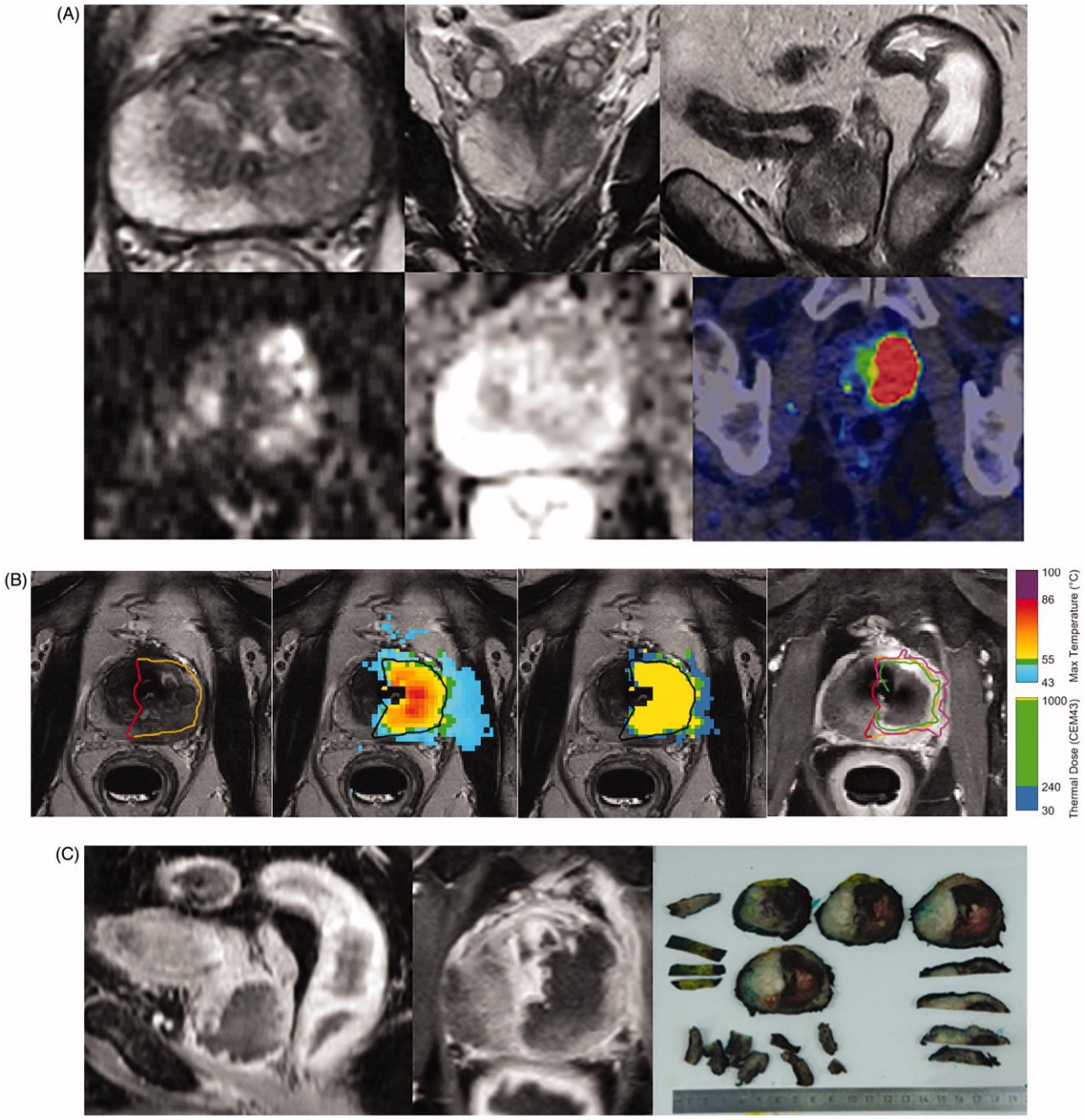

Treatment details and pathological evaluation with H&E staining

Patient 4 underwent lesion-targeted TULSA, with sonication and MRI times of 14 and 130 minutes, respectively. The MRI-thermometry derived maximum temperature and thermal dose maps showed a homogeneous and continuous cytocidal heating pattern extending into the prostate capsule and

completely containing the targeted predefined region including the index tumor (Figure 2b.). The 3-week-NPV covered the targeted tumor without any enhancement observed inside the NPV indicating complete devascularization of the targeted region (Figure 2c). Further, the RALP-procedure was uneventful without treatment related complications.

H&E stained analysis of the RALP specimen from the same patient indicated a distinct round-shaped focus of morphologically viable adenocarcinoma **in two consecutive slides 5 mm apart from each other**, retaining nuclear and cytological details and resembling predominantly Gleason pattern 4 disease. The focus was situated within the ablated area, surrounded by CNZ (Figure 3). The surrounding CNZ was characterized by retention of cellular outline but loss of cytoplasmic and nuclear details, and the presence of hemorrhage and loosely woven collagen.

Figure 3. Histological analysis of prostatic thermal injury. An annotated axial H&E-stained whole-mount slide mid from the RALP specimen of the patient four showing the complete irreversible cell death inside the red boundary (CNZ) and margin zone between red and blue boundaries (MZ). Magnification H&E images from thermally-fixed area show well preserved morphology of Gleason 4 adenocarcinoma.

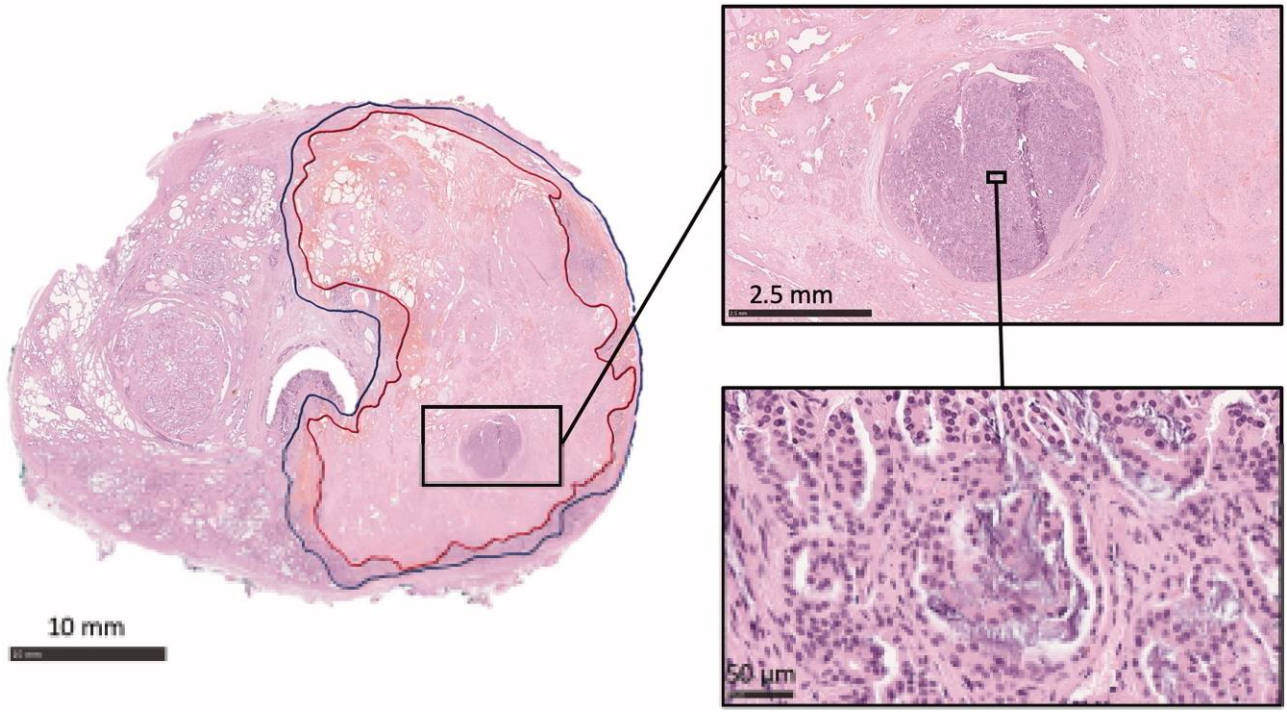

Interestingly, the region that appeared viable on H&E staining was located in the zone where the highest temperatures were reached based on MRI-thermometry data, and was within a region of uniformly non-enhancing tissue on contrast-enhanced MRI. Quantitatively, the closest distance from the edge of the thermally-fixed region to the urothelium of the urethra was 8 mm, matching the 8 mm distance from the urothelium of the urethra to the maximum temperatures of 83.3°C on MRI-thermometry. Furthermore, this patient differed from the other five study patients based on the finding that this patient had the fastest heat response of all treatments (time from start of heating to peak: 12°C/min vs median 7°C/min (range: 5.2-10)) possibly explaining occurrence of thermal fixation in this case.

Immunohistochemistry of areas suspected to present thermal fixation

IHC revealed that neither the apparently viable region nor the surrounding CNZ stained positively for cytokeratin 8, as assessed by Cam5.2 antibody (Figure 4). Conversely, both the untreated benign region and apparent residual carcinoma just outside the ablated area were cytokeratin 8 positive (Figure 4). These observations suggest that negative cytokeratin 8 staining against a background of positive-staining untreated tissue can identify both thermally-fixed and thermally-necrosed cells.

Figure 4. Immunohistochemical staining patterns of different prostatic regions after thermal injury. Two parallel HE-stained macro-sections from mid-prostate are shown from the same patient. High magnification images from benign-untreated region, coagulative necrosis zone (CNZ), thermally-fixed region (TF) and residual carcinoma (RC) with different stainings are shown below, and the defined regions are indicated with squares in the low magnification macro images. Note that there is a loss of cytokeratin 8 (Cam5.2) and AMACR staining in both CNZ and TF regions. A strong extracellular staining for vWF is seen in CNZ, while the staining is restricted to vessels in other regions. AR and p16 are weakly positive in CNZ and TF regions but virtually more abundant in RC region. Scale bar 10 mm for macro-sections, 0.5 mm for high magnification images.

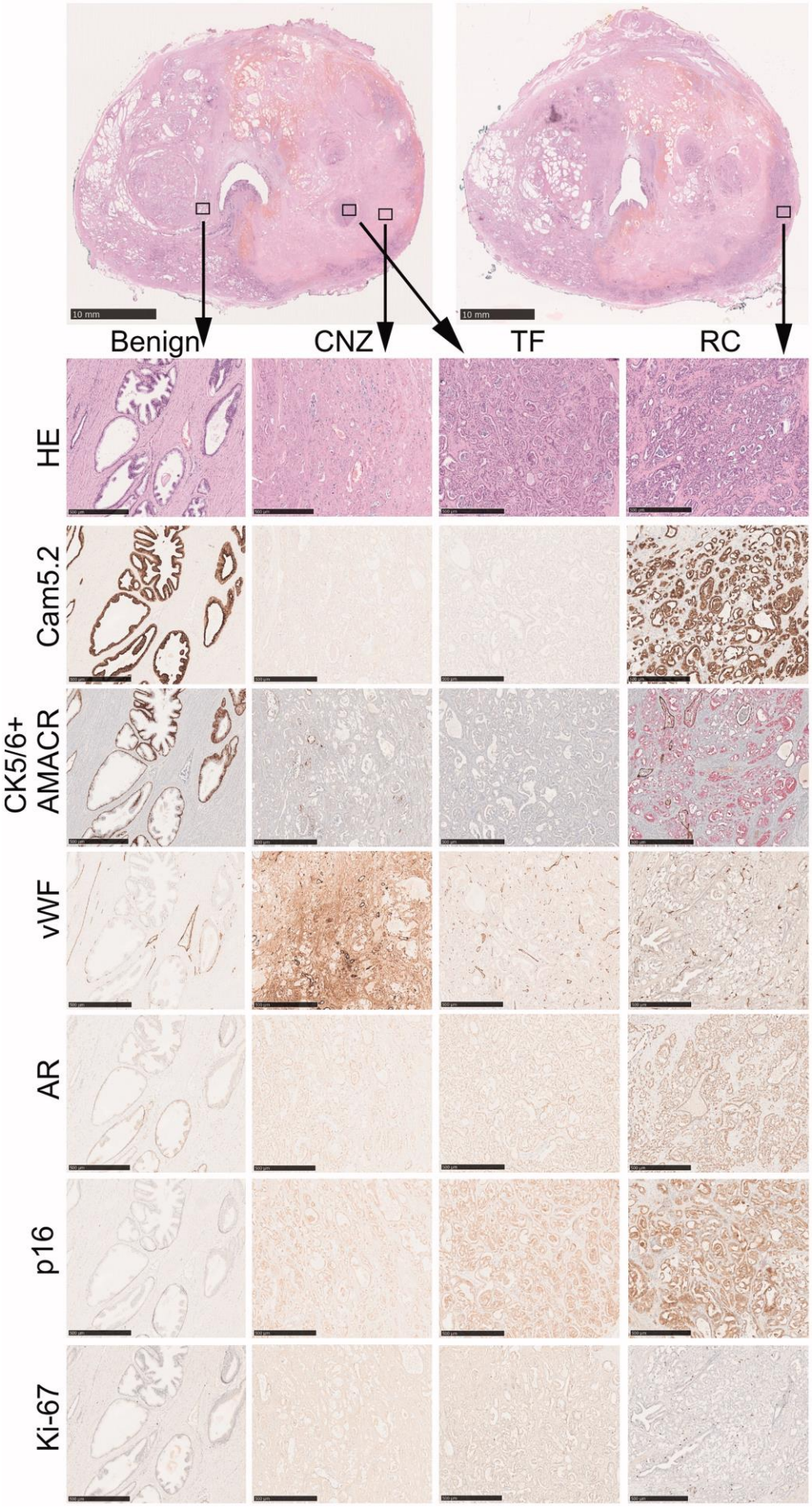
10 mm
10 mm
Benign
CNZ
TF
RC
HE
Cam5.2
CK5/6+
AMACR
vWF
AR
p16
Ki-67

The patient presented abnormally excessive vWF immunostaining in the CNZ and MZ due to thermally injured blood vessels and leakage of plasma and platelets into the interstitial tissue. Both the apparently viable and untreated regions on H&E staining presented normal vWF immunostaining (Figure 4). These observations suggest a lack of vascular damage within thermally-fixed regions.

The final histopathological report of the experienced uropathologist concluded that the cells that appeared viable on H&E staining were in fact non-viable and had died by thermal fixation. The most significant evidence was the negative staining with cytokeratin 8 (Cam 5.2) and AMACR antibodies, which were both positive in the residual carcinoma outside the targeted region near neurovascular bundle. To our surprise, p16 and androgen receptor stainings were weakly positive in the thermally-fixed cells but more evident in the residual carcinoma outside the treated region. Ki-67 staining showed the highest number of positively stained cells within untreated residual carcinoma, with a small number of Ki-67 positive cells also found in the thermally-fixed region, while benign tissue and CNZ were virtually negative.

DISCUSSION

Here we presented a case from a treat-and resect clinical trial where the study patient presented with apparently viable cells in initial H&E stained histology of their RP specimen after TULSA. However, analysis of MRI-thermometry, 3-week post-TULSA NPV, and immunohistochemistry concluded that in fact these cells were severely damaged and non-viable, having undergone thermal fixation. In particular, loss of cytokeratin 8 staining was indicative of severe cellular damage in both thermally-fixed and thermally-necrosed regions, and a lack of von Willebrand Factor enhancement

suggested that fixation involves cellular damage without vascular effects. While we had a small number of patients (due to the lack of patient benefit in a treat-and-resect study), our detailed description of staining outcomes in whole-mount tissues acquired three weeks after treatment with a novel ablation device provides valuable confirmation and extension of the limited available literature on thermal fixation. These observations offer important guidance for pathologists reviewing an increasing number of post-ablation histological specimens.

Table 1 summarizes our comprehensive literature search comprising all original articles discussing at least one case of thermally-fixed tissue after thermal ablation. In these studies, initial H&E stained histopathological evaluation of ablation efficacy consistently revealed a region of tissue that appeared morphologically viable within a larger ablated region, suggesting untreated or surviving viable tissue. Several methods have been exploited to confirm that these regions represent thermally-fixed cells with severely damaged non-viable tissue, including supravital stains (TTC and NADH), IHC (in prostate; panCK, CK8, vWF, Ki-67), electron microscopy, and fluorescence microscopy (Table 1). However, some of these methods are not routinely available or not feasible in clinical practice, such as electron microscopy. Furthermore, supravital stainings can only be performed on fresh tissue specimens, while fluorescence microscopy has not been validated in human tissue specimens.

In addition to our current study there are only 5 human *in vivo* studies reporting thermally-fixed cells after thermal ablation: two in the prostate (6 cases after HIFU and 4 cases after focal laser ablation), two in the liver (4 cases after radiofrequency ablation and 1 case after HIFU) and one in the breast (11 cases after HIFU). **There are no previous reports on thermal fixation for in vivo human prostate using transurethral ultrasound therapy, which has distinct patterns of**

thermal dose deposition and histological damage due to the use of continuous heating with an unfocused ultrasound beam (as opposed to a series of brief small volume exposures in HIFU).

Specific to prostate tissue, two other *in vivo* studies and one *in vitro* study have reported thermally-fixed cells in human prostates after thermal ablation, and one additional *in vivo* study reported findings in canine prostates. In both *in vivo* human studies, cytokeratin 8 staining was utilized for detecting non-viable dead tissue [16,36]. Van Leenders et al. [16] demonstrated an apparent concordance between cytokeratin 8 negative prostate tissue inside ablated area and ultrastructural electron microscopy changes consistent with necrosis. Based on our results and the conclusions of these studies, cytokeratin 8, as detected by Cam5.2 antibody, appears more sensitive for detection of necrosis than H&E staining, identifying cells that are non-viable despite retaining normal morphologic features on H&E. **Following transurethral ultrasound ablation in canine prostates, Boyes el al [17] observed a TFZ located in the central area of the CNZ where the highest temperature is likely to occur, and more prominent when large target boundaries result in faster temperature rise and higher temperatures enabling formation of thermal fixation. In our study, a distinct TFZ was distinguishable in only one patient, but was similarly located within the CNZ in the region with the highest maximum temperature. This patient also had the most rapid temperature rise among the six study patients, possibly related to a large intended treatment volume as suggested by Boyes et al [17].**

Besides traditional therapies (RP, RT, brachytherapy), FTs have emerged as a potential therapeutic option in localized PCa with the main purpose of selective tumor ablation with equivalent oncological control, reduced toxicity, and improved functional outcomes. Remaining challenges for organ-sparing ablation strategies include determining how to ensure oncological safety and how to optimize follow-up of oncological outcomes in both in-field and out-of-field regions. Apart from

imaging and PSA, consensus guidelines recommend using follow-up biopsy specimens from the ablated region to assess treatment outcome [6]. However, histopathological assessment of biopsy specimens after thermal ablation may be confounded by thermally-fixed cells that appear to be viable on H&E staining. The prevalence of thermally-fixed tissue in prostate biopsy specimens after thermal ablation is unknown. Furthermore, it is not known how long thermally-fixed cells can retain apparently viable morphology after thermal ablation. In liver tissue, the appearance of thermal fixation can remain up to at least 14 months post-ablation [32]. If this finding applies also in the prostate, one could speculate on the possibility of detecting thermally-fixed non-viable cells in post-ablation biopsy specimens. This would have important clinical implications, since guidelines suggest the use of serial follow-up biopsies from the ablated area as a defining component of surveillance after prostate focal therapy [6,53].

Although heat exposure is increasingly being utilized in PCa-management, both the phenomenon of thermal fixation and its incidence are poorly known in clinical practice. Currently there is no standard method to determine the viability of heat-fixed cells, which may lead to incorrect diagnosis of treatment failure when pathologists assess biopsy specimens from thermally ablated regions. Several supplemental histopathological examinations have suggested that thermally-fixed cells represent non-viable dead tissue, including supravital stains, autofluorescence, electron microscopy and IHC from apparently viable regions suspected to present thermal fixation. In particular, the results of our study and others in human prostate cancer have demonstrated that a loss of cytokeratin 8 staining in glandular epithelium after thermal ablation indicates severe cellular damage, and correlates with necrosis in ultrastructural examinations (Table 1). **However, it is important to note that while Cam5.2 has primary reactivity with cytokeratin 8 it is also reactive with cytokeratin 7, yet there is no published literature about the utility of cytokeratin**

8 antibodies other than Cam5.2 in detecting thermally-fixed cells. Since the negative staining is presumably due to loss of antigenicity for Cam5.2 antibody rather than true lack of cytokeratin 8 itself, this pitfall needs to be considered in clinical diagnosis of post-ablation histological specimens. A loss of AMACR staining in thermally-fixed cells may also be helpful, but cannot be considered ground truth as approximately 10% of adenocarcinomas appear AMACR negative. **While these stains offer practical tools for assessing cells that appear viable within regions of intense thermal damage, there is still a need for further development, standardization, and utilization of histological markers of thermal fixation.**

CONCLUSION

Thermally-fixed cells can appear viable due to sustained morphological detail on H&E staining after thermal ablation. Interpretation of prostate specimens after thermal ablation may suggest treatment failure, if this effect is not recognized and ancillary immunohistochemistry performed. Based on the previous literature and the current study, cytokeratin 8 (Cam5.2) and AMACR staining appear practical and reliable tools for distinguishing thermally-fixed non-viable cells from viable cells.

REFERENCES

[1] Bill-Axelson A, Holmberg L, Garmo H, Rider JR, Taari K, Busch C, et al. Radical prostatectomy or watchful waiting in early prostate cancer. New England journal of medicine 2014;370 932-42.

[2] Wilt TJ, Jones KM, Barry MJ, Andriole GL, Culkin D, Wheeler T, et al. Follow-up of Prostatectomy versus Observation for Early Prostate Cancer. New England journal of medicine 2017;377 132-42.

[3] Hamdy FC, Donovan JL, Lane JA, Mason M, Metcalfe C, Holding P, et al. 10-Year Outcomes after Monitoring, Surgery, or Radiotherapy for Localized Prostate Cancer. New England journal of medicine 2016;375 1415-24.

[4] Donovan JL, Hamdy FC, Lane JA, Mason M, Metcalfe C, Walsh E, et al. Patient-reported outcomes after monitoring, surgery, or radiotherapy for prostate cancer. New England journal of medicine 2016;375 1425-37.

[5] Sanda MG, Dunn RL, Michalski J, Sandler HM, Northouse L, Hembroff L, et al. Quality of life and satisfaction with outcome among prostate-cancer survivors. New England journal of medicine 2008;358 1250-61.

[6] van der Poel, Henk G, van den Bergh, Roderick CN, Briers E, Cornford P, Govorov A, Henry AM, et al. Focal therapy in primary localised prostate cancer: the European Association of Urology position in 2018. European Urology 2018;74 84-91.

[7] Valerio M, Cerantola Y, Eggener SE, Lepor H, Polascik TJ, Villers A, et al. New and established technology in focal ablation of the prostate: a systematic review. European Urology 2017;71 17-34.

[8] Woodrum DA, Gorny KR, Mynderse LA. Mr-guided Prostate Interventions. Topics in Magnetic Resonance Imaging 2018;27 141-51.

[9] Ahmed HU, Bosaily AE, Brown LC, Gabe R, Kaplan R, Parmar MK, et al. Diagnostic accuracy of multi-parametric MRI and TRUS biopsy in prostate cancer (PROMIS): a paired validating confirmatory study. Lancet 2017;389 815-22.

[10] Kasivisvanathan V, Rannikko AS, Borghi M, Panebianco V, Mynderse LA, Vaarala MH, et al. MRI-targeted or standard biopsy for prostate-cancer diagnosis. New England journal of medicine 2018;378 1767-77.

[11] Ramsay E, Mougenot C, Staruch R, Boyes A, Kazem M, Bronskill M, et al. Evaluation of focal ablation of magnetic resonance imaging defined prostate cancer using magnetic resonance imaging controlled transurethral ultrasound therapy with prostatectomy as the reference standard. The Journal of Urology 2017;197 255-61.

[12] Chopra R, Colquhoun A, Burtnyk M, N'djin WA, Kobelevskiy I, Boyes A, et al. MR imaging–controlled transurethral ultrasound therapy for conformal treatment of prostate tissue: Initial feasibility in humans. Radiology 2012;265 303-13.

[13] Chin JL, Billia M, Relle J, Roethke MC, Popeneciu IV, Kuru TH, et al. Magnetic resonance imaging–guided transurethral ultrasound ablation of prostate tissue in patients with localized prostate cancer: a prospective phase 1 clinical trial. European Urology 2016;70 447-55.

[14] Ross AB, Diederich CJ, Nau WH, Gill H, Bouley DM, Daniel B, et al. Highly directional transurethral ultrasound applicators with rotational control for MRI-guided prostatic thermal therapy. Physics in Medicine & Biology 2004;49 189.

[15] Chu KF, Dupuy DE. Thermal ablation of tumours: biological mechanisms and advances in therapy. Nature Reviews: Cancer 2014;14 199-208.

[16] Van Leenders G, Beerlage HP, Ruijter ET, De La Rosette J, Van De Kaa, C A. Histopathological changes associated with high intensity focused ultrasound (HIFU) treatment for localised adenocarcinoma of the prostate. Journal of Clinical Pathology 2000;53 391-4.

[17] Boyes A, Tang K, Yaffe M, Sugar L, Chopra R, Bronskill M. Prostate tissue analysis immediately following magnetic resonance imaging guided transurethral ultrasound thermal therapy. Journal of Urology 2007;178 1080-5.

[18] Burtnyk M, Hill T, Cadieux-Pitre H, Welch I. Magnetic resonance image guided transurethral ultrasound prostate ablation: a preclinical safety and feasibility study with 28-day followup. Journal of Urology 2015;193 1669-75.

[19] Ishihara Y, Calderon A, Watanabe H, Okamoto K, Suzuki Y, Kuroda K, et al. A precise and fast temperature mapping using water proton chemical shift. Magnetic resonance in medicine 1995;34 814-23.

[20] Ramsay E, Mougenot C, Köhler M, Bronskill M, Klotz L, Haider MA, et al. MR thermometry in the human prostate gland at 3.0 T for transurethral ultrasound therapy. Journal of Magnetic Resonance Imaging 2013;38 1564-71.

[21] Siddiqui K, Chopra R, Vedula S, Sugar L, Haider M, Boyes A, et al. MRI-guided Transurethral Ultrasound Therapy of the Prostate Gland Using Real-time Thermal Mapping: Initial Studies. Urology 2010;76 1506-11.

[22] Chopra R, Tang K, Burtnyk M, Boyes A, Sugar L, Appu S, et al. Analysis of the spatial and temporal accuracy of heating in the prostate gland using transurethral ultrasound therapy and active MR temperature feedback. Physics in Medicine & Biology 2009;54 2615.

[23] Böni RA, Sulser T, Jochum W, Romanowski B, Debatin JF, Krestin GP. Laser ablation-induced changes in the prostate: findings at endorectal MR imaging with histologic correlation. Radiology 1997;202 232-6.

[24] Rouvière O, Lyonnet D, Raudrant A, Colin-Pangaud C, Chapelon JY, Bouvier R, et al. MRI appearance of prostate following transrectal HIFU ablation of localized cancer. European Urology 2001;40 265-74.

[25] Bomers JGR, Cornel EB, Futterer JJ, Jenniskens SFM, Schaafsma HE, Barentsz JO, et al. MRI-guided focal laser ablation for prostate cancer followed by radical prostatectomy: correlation of treatment effects with imaging. World Journal of Urology 2017;35 703-11.

[26] Rosset R, Bratan F, Crouzet S, Tonoli-Catez H, Mège-Lechevallier F, Gelet A, et al. Can pre- and postoperative magnetic resonance imaging predict recurrence-free survival after whole-gland high-intensity focused ablation for prostate cancer?. European Radiology 2017;27 1768-75.

[27] Biermann K, Montironi R, Lopez-Beltran A, Zhang S, Cheng L. Histopathological findings after treatment of prostate cancer using high-intensity focused ultrasound (HIFU). Prostate 2010;70 1196-200.

[28] Germer C, Isbert CM, Albrecht D, Ritz JP, Schilling A, Roggan A, et al. Laser-induced thermotherapy for the treatment of liver metastasis. Surgical Endoscopy 1998;12 1317-1325.

[29] Bhowmick S, Coad JE, Swanlund DJ, Bischof JC. In vitro thermal therapy of AT-1 Dunning prostate tumours. International Journal of Hyperthermia 2004;20 73-92.

[30] Hennings L, Kaufmann Y, Griffin R, Siegel E, Novak P, Corry P, et al. Dead or alive? Autofluorescence distinguishes heat-fixed from viable cells. International Journal of Hyperthermia 2009;25 355-63.

[31] Stafford RJ, Shetty A, Elliott AM, Klumpp SA, McNichols RJ, Gowda A, et al. Magnetic resonance guided, focal laser induced interstitial thermal therapy in a canine prostate model. Journal of Urology 2010;184 1514-1520.

[32] Coad JE, Kosari K, Humar A, Sielaff TD. Radiofrequency ablation causes ‘thermal fixation’of hepatocellular carcinoma: a post-liver transplant histopathologic study. Clinical Transplantation 2003;17 377-84.

[33] Coad JE. Thermal fixation: a central outcome of hyperthermic therapies 2005;5698 15-23.

[34] He X, McGee S, Coad JE, Schmidlin F, Iaizzo PA, Swanlund DJ, et al. Investigation of the thermal and tissue injury behaviour in microwave thermal therapy using a porcine kidney model. International Journal of Hyperthermia 2004;20 567-93.

[35] Courivaud F, Kazaryan AM, Lund A, Orszagh VC, Svindland A, Marangos IP, et al. Thermal fixation of swine liver tissue after magnetic resonance-guided high-intensity focused ultrasound ablation. Ultrasound in Medicine & Biology 2014;40 1564-77.

[36] Lindner U, Lawrentschuk N, Weersink RA, Davidson SR, Raz O, Hlasny E, et al. Focal laser ablation for prostate cancer followed by radical prostatectomy: validation of focal therapy and imaging accuracy. European Urology 2010;57 1111-4.

[37] Wu F, Wang Z, Cao Y, Xu Z, Zhou Q, Zhu H, et al. Heat fixation of cancer cells ablated with high-intensity–focused ultrasound in patients with breast cancer. The American Journal of Surgery 2006;192 179-84.

[38] Beat M Künzli Paolo Abitabile Christoph A Maurer. Radiofrequency ablation of liver tumors: Actual limitations and potential solutions in the future. World Journal of Hepatology 2011;3 8-14.

[39] Leslie TA, Kennedy JE, Illing RO, Ter Haar GR, Wu F, Phillips RR, et al. High-intensity focused ultrasound ablation of liver tumours: can radiological assessment predict the histological response?. The British Institute of Radiology 2008;81 564-71.

[40] van Vulpen M, Raaymakers BW, de Leeuw AA, van de Kamer, Jeroen B, Jeroen A, van Moorselaar R, et al. Prostate perfusion in patients with locally advanced prostate carcinoma treated with different hyperthermia techniques. Journal of Urology 2002;168 1597-602.

[41] Sapareto SA, Dewey WC. Thermal dose determination in cancer therapy. International Journal of Radiation Oncology • Biology • Physics 1984;10 787-800.

[42] Dewhirst MW, Viglianti BL, Lora-Michiels M, Hanson M, Hoopes PJ. Basic principles of thermal dosimetry and thermal thresholds for tissue damage from hyperthermia. International journal of hyperthermia 2003;19 267-94.

[43] Damianou C, Hynynen K. The effect of various physical parameters on the size and shape of necrosed tissue volume during ultrasound surgery. The Journal of the Acoustical Society of America 1994;95 1641-9.

[44] Fan X, Hynynen K. Ultrasound surgery using multiple sonications—treatment time considerations. Ultrasound in Medicine & Biology 1996;22 471-82.

[45] Yarmolenko PS, Moon EJ, Landon C, Manzoor A, Hochman DW, Viglianti BL, et al. Thresholds for thermal damage to normal tissues: an update. International Journal of Hyperthermia 2011;27 320-43.

[46] Li GC, Mivechi NF, Weitzel G. Heat shock proteins, thermotolerance, and their relevance to clinical hyperthermia. International journal of hyperthermia 1995;11 459-88.

[47] Borrelli MJ, Thompson LL, Cain CA, Dewey WC. Time-temperature analysis of cell killing of BHK cells heated at temperatures in the range of 43.5 C to 57.0 C. International Journal of Radiation Oncology* Biology* Physics 1990;19 389-99.

[48] Field SB, Morris CC. The relationship between heating time and temperature: its relevance to clinical hyperthermia. Radiotherapy and Oncology 1983;1 179-86.

[49] Majno G, Joris I. Apoptosis, oncosis, and necrosis. An overview of cell death. The American journal of pathology 1995;146 3-15.

[50] Vykhodtseva N, Mcdannold N, Martin H, Bronson RT, Hynynen K. Apoptosis in ultrasound-produced threshold lesions in the rabbit brain. Ultrasound in Medicine & Biology 2001;27 111-7.

[51] Wall MS, Deng X, Torzilli PA, Doty SB, O'Brien SJ, Warren RF. Thermal modification of collagen. Journal of shoulder and elbow surgery 1999;8 339-44.

[52] Wright NT, Humphrey JD. Denaturation of collagen via heating: an irreversible rate process. Annual Review of Biomedical Engineering 2002;4 109-28.

[53] Tay KJ, Amin MB, Ghai S, Jimenez RE, Kench JG, Klotz L, et al. Surveillance after prostate focal therapy. World Journal of Urology 2019;37 397-407.

APPENDIX

Table S1. Antibodies used in immunohistochemistry (IHC)

Antibody	**Clone**	**Vendor**	**Dilution**
AR (androgen receptor)	AR27	Novocastra	1:10
CK5/6 + Racemase/AMACR	D5&16B4 + 13H4	Ventana/Zeta Corp	Ventana disp + 1:200 prep kit
CKCam5.2	Cam5.2	Becton Dick	1:10
Ki-67	30-9	Ventana/Roche	*
p16	E6H4	Ventana/Roche	*
von Willebrandt F VIII	polyclonal	Dako	1:1000

* All Ventana's antibodies were used as manufacturer's standardized dispenser dilutions.